310:
Inferring lightning-channel geometry from polarimetry of VHF radio emissions

Abram R. Jacobson*, Robert H. Holzworth (Univ. of Washington, Seattle WA, USA)
Xuan-Min Shao (Los Alamos National Laboratory, Los Alamos NM, USA)

*corresponding author: abramj@u.washington.edu

Introduction(1)

Certain intracloud lightning discharges emit energetic, multi-microsecond pulsetrains of radio noise. Observations of this distinctive form of lightning date from 1980 and have involved both ground-based and satellite-based radio recording systems. The underlying intracloud lightning discharges have been referred to as "Narrow Bipolar Pulses", "Narrow Bipolar Events", and "Compact Intracloud Discharges". An important discriminant for this species of radio emission is that, in the range above ~ 30 MHz, it consists of several microseconds of intense radio noise. Two additional, contextual discriminants for this species of radio emission are that the accompanying light emission is relatively low, and that there is little if any leader activity preceding the powerful emission.

When the intracloud emission is viewed from a satellite, each radio pulsetrain is received both from a direct lightning-to-satellite path, and after some delay, from a path via ground. Thus one recording of the radio emission, if of sufficient length, contains the "view" of the intracloud emission from two different angles. One view is of radiation exiting the emitter into the upper hemisphere, the other for radiation exiting into the lower hemisphere. However, the propagation conditions are similar, except that one path includes a ground reflection, while the other does not.

Introduction(2)

One would normally expect a stereoscopic double view of the "same" emission process to provide two almost congruent time series, one delayed from the other, and also differing due to the different propagation effects along the two signal paths, namely, the ground reflection. We present somewhat unexpected results on this matter, using recordings from the FORTE satellite at a passband 118-141 MHz, with simultaneous data at 26-49 MHz. We find that the 118-141 MHz pulsetrain's detailed time-dependence is completely uncorrelated between the two views of the process. We examine statistics of the 118-141 MHz pulsetrain's integrated power and show that the power emitted into the lower hemisphere, on average, exceeds the power emitted into the upper hemisphere. Finally, we examine statistical measures of the amplitude distribution and show that the 118-141 MHz signal emitted downward is slightly more dominated by discrete, temporally-narrow impulses than is the signal emitted upward.

This unexpected feature of the powerful intracloud VHF emissions implies that a stereoscopic double view is not possible. The down-going emission is sufficiently different from the up-going emission that the supposition underlying a stereoscopic method does not apply.

Why is this happening?

Conclusions

(a) The FORTE high-band (130 MHz) reveals that each pulsetrain contains numerous quasi-discrete, narrow peaks. At 130 MHz, we can be sure that this oberved property is not an artifact of residual ionospheric dispersion and mode doubling. (At 38 MHz, these effects tend to blur such peaks.)

(b) The quasi-discrete, narrow peaks in the pulsetrains are essentially uncorrelated between the two views of the discharge (direct path, and path via ground). Thus, we have avoided calling the signal arriving from the ground the "reflected signal", because that implies that otherwise it is the same signal as arrives on the direct path. It is true that there is a reflection at the ground, but we have no evidence that the "reflected" signal behaves like a replica of the direct signal.

(c) The 130-MHz energy arriving via the ground shows a statistically significant tendency to exceed the energy arriving along the direct path. This is not the case at the low band, 38 MHz.

(d) The quasi-discrete peaks in the pulsetrain cause the amplitude distribution to be leptokurtic; the signal arriving via ground is slightly more leptokurtic.

(e) The pulsetrain arriving via the ground has 1-2 microsec additional width (based on energy), relative to the pulsetrain arriving on the direct path.

(f) The peaks within a pulsetrain in some cases appear to occur quasi-regularly, but this is not consistent even in the minority of cases when it occurs. Quasi-regular repetition does not appear in the majority of records.

(g) One can speculate that two processes might create some of the troubling dissimilarity between the pulsetrains along the different paths: Spatially extended emission region, and relativistic "headlighting".

Table 1: Selected data sets

parameter	less stringent data set	more stringent data set
130-MHz contrast ratio	> 20	> 100
130-MHz lagged-peak SNR	> 5	> 20
130-MHz 1-microsec-avg ERP	> 0.2 kW	> 2 kW
130-MHz interpulse separation	> 20 microsec	> 20 microsec
130-MHz autocor 1/e width	> 2 microsec	> 2 microsec
number of events in data set	3798	856

Table 2: Fraction of recordings with energy ratio (via ground)/(direct) > 1

surface / frequency band	contrast >20, snr >5, ERP >0.2 kW	contrast >100, snr >20, ERP >2kW
land / 130 MHz	0.14	0.24
coast/ 130 MHz	0.40	0.59 *
sea/ 130 MHz	0.54 *	0.65 *
land/ 38 MHz	0.09	0.14
coast/ 38 MHz	0.33	0.41
sea/ 38 MHz	0.34	0.45

Acknowledgement: Two authors (ARJ, RH) worked on this project with support from the U. S. Defense Advanced Research Projects Agency's NIMBUS program.

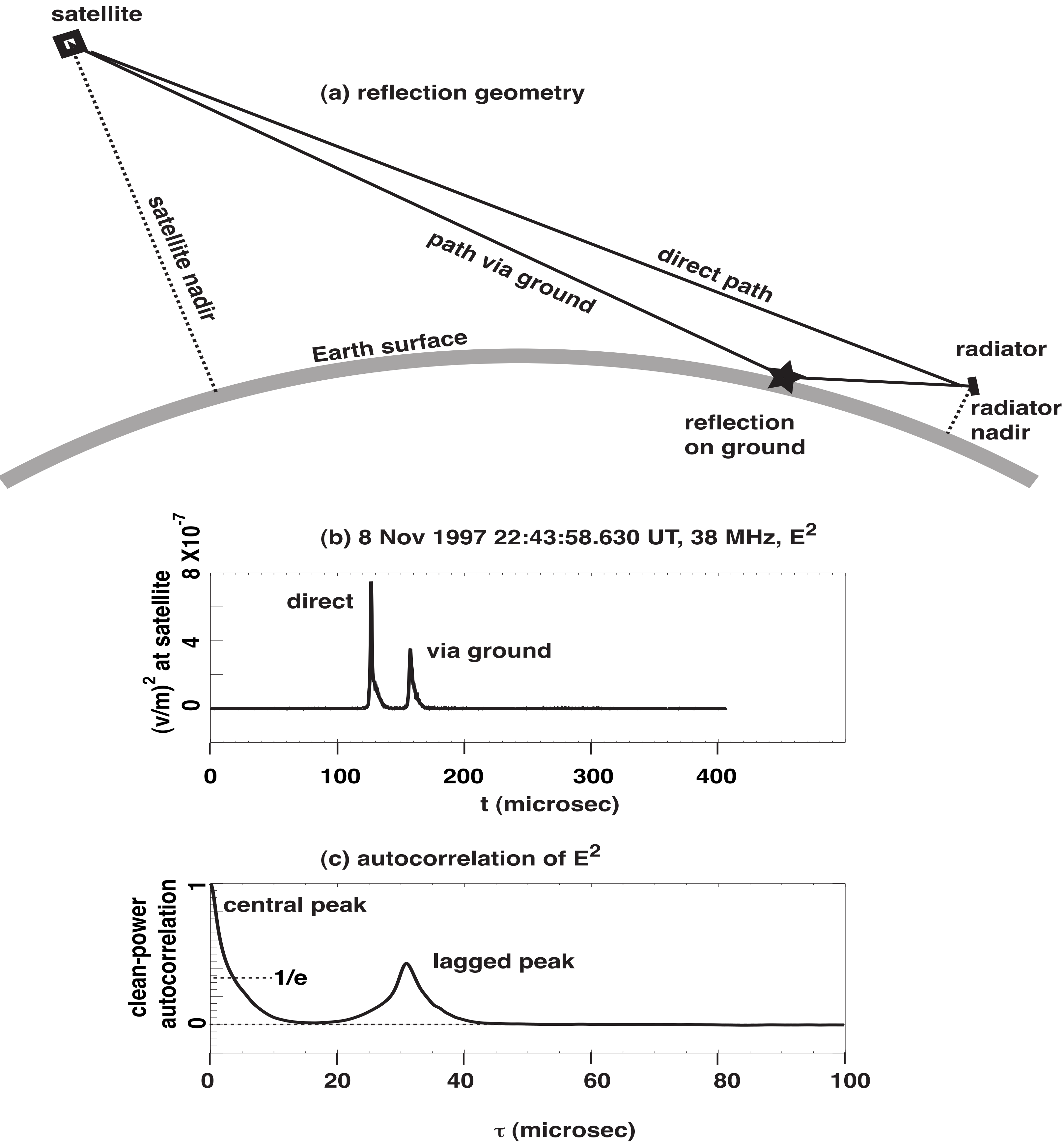

Figure 1: (a) Scheme of viewing geometry. Lightning above ground is viewed both along a direct path and via the ground, which acts as a good reflector for VHF. (b) Sequence of 1-microsec-averaged E^2 showing two pulses recorded by FORTE satellite. (c) Lagged autocorrelation function of E^2 from this signal.

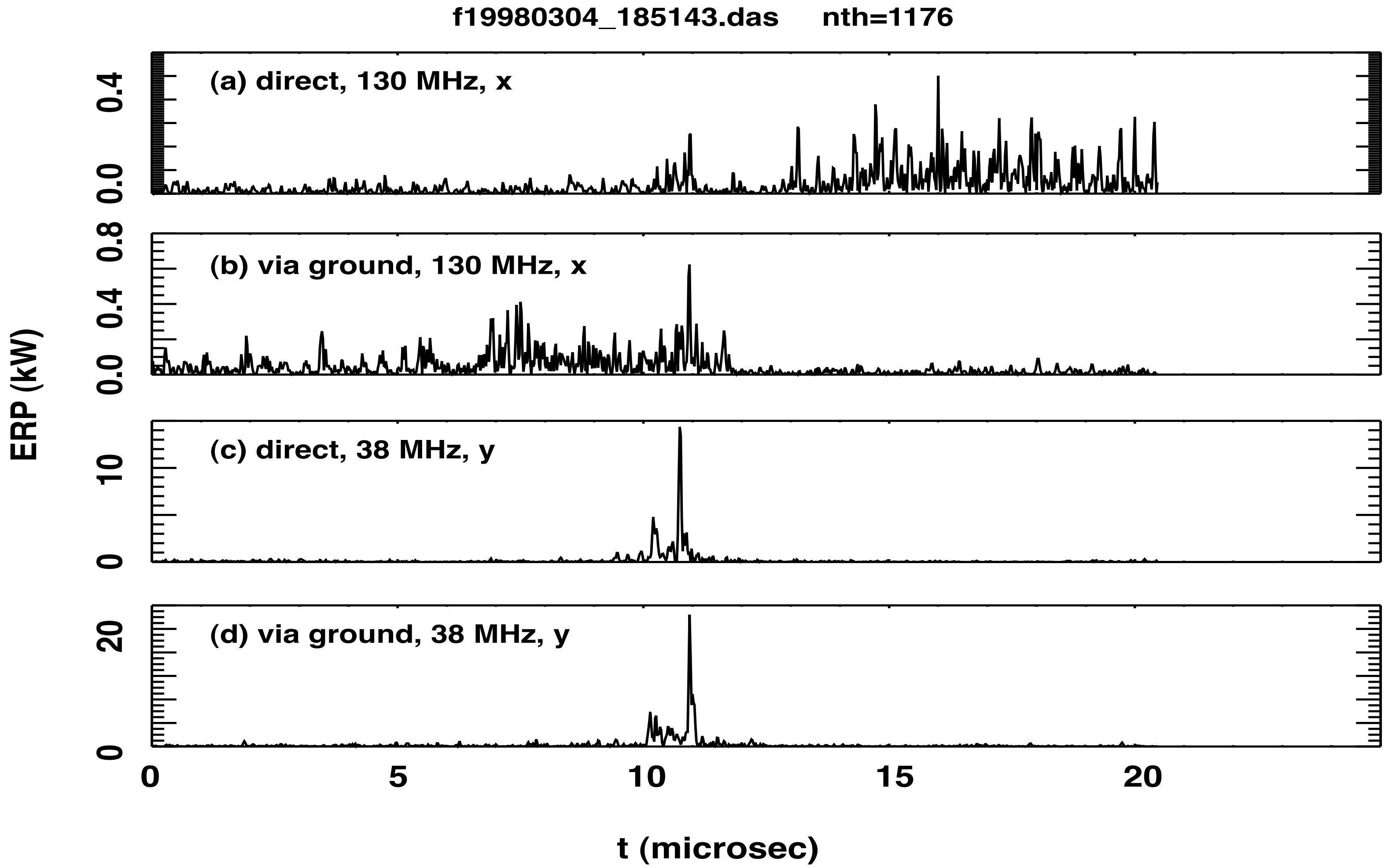

Figure 2: Dechirped, prewhitened effective radiated power (ERP) versus t, for a typical *low-energy, narrow* intracloud VHF pulse. This pulse is typical of those *not selected* for the present study. (a) Direct path, 130 MHz, antenna x. (b) Via ground, 130 MHz, antenna x. (c) Direct path, 38 MHz, antenna y. (d) Via ground, 38 MHz, antenna y.

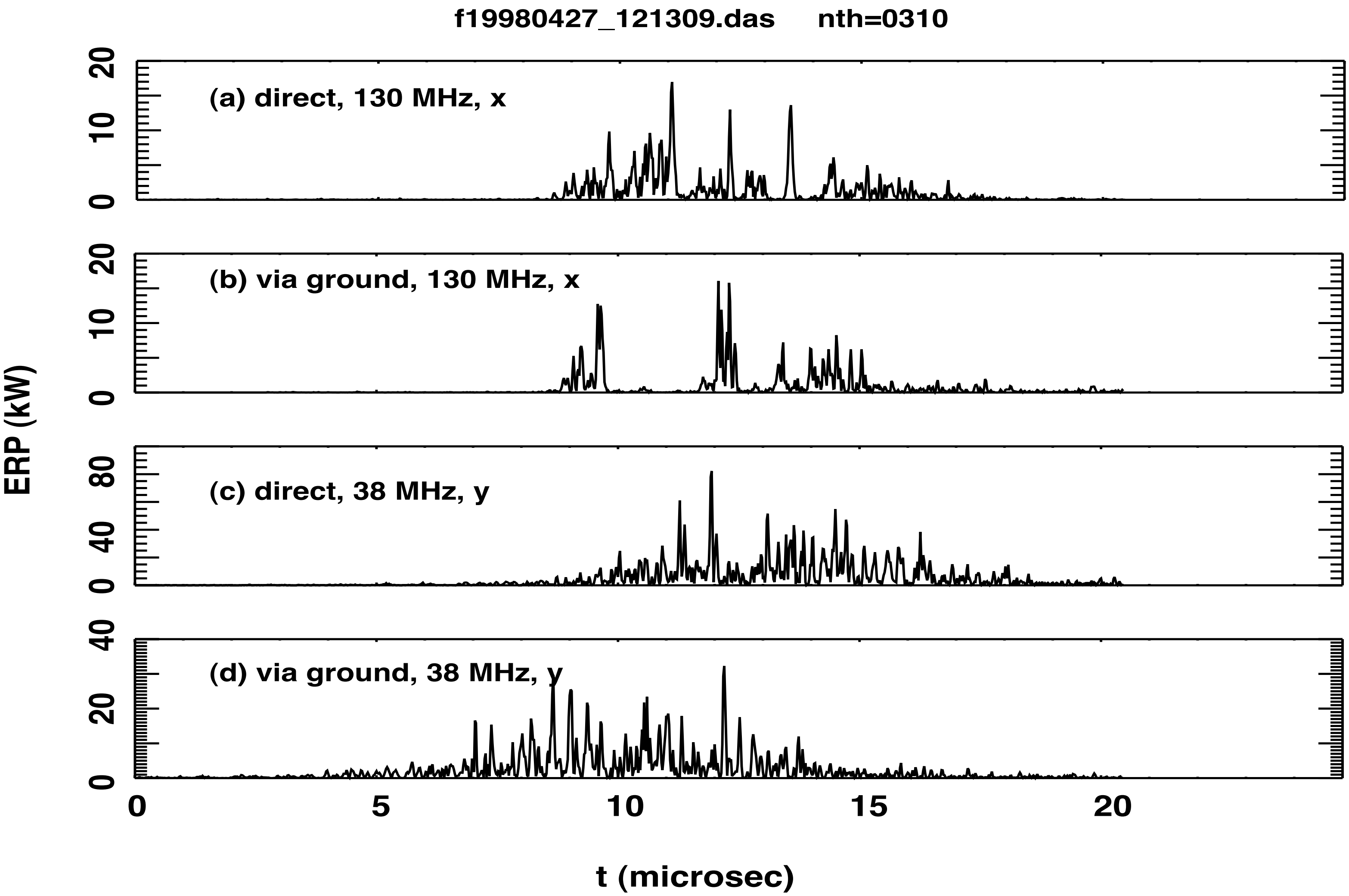

Figure 3: Dechirped, prewhitened effective radiated power (ERP) versus t, for a typical *high-energy, wide* intracloud VHF pulse. This pulse is typical of those selected for the present study. (a) Direct path, 130 MHz, antenna x. (b) Via ground, 130 MHz, antenna x. (c) Direct path, 38 MHz, antenna y. (d) Via ground, 38 MHz, antenna y.

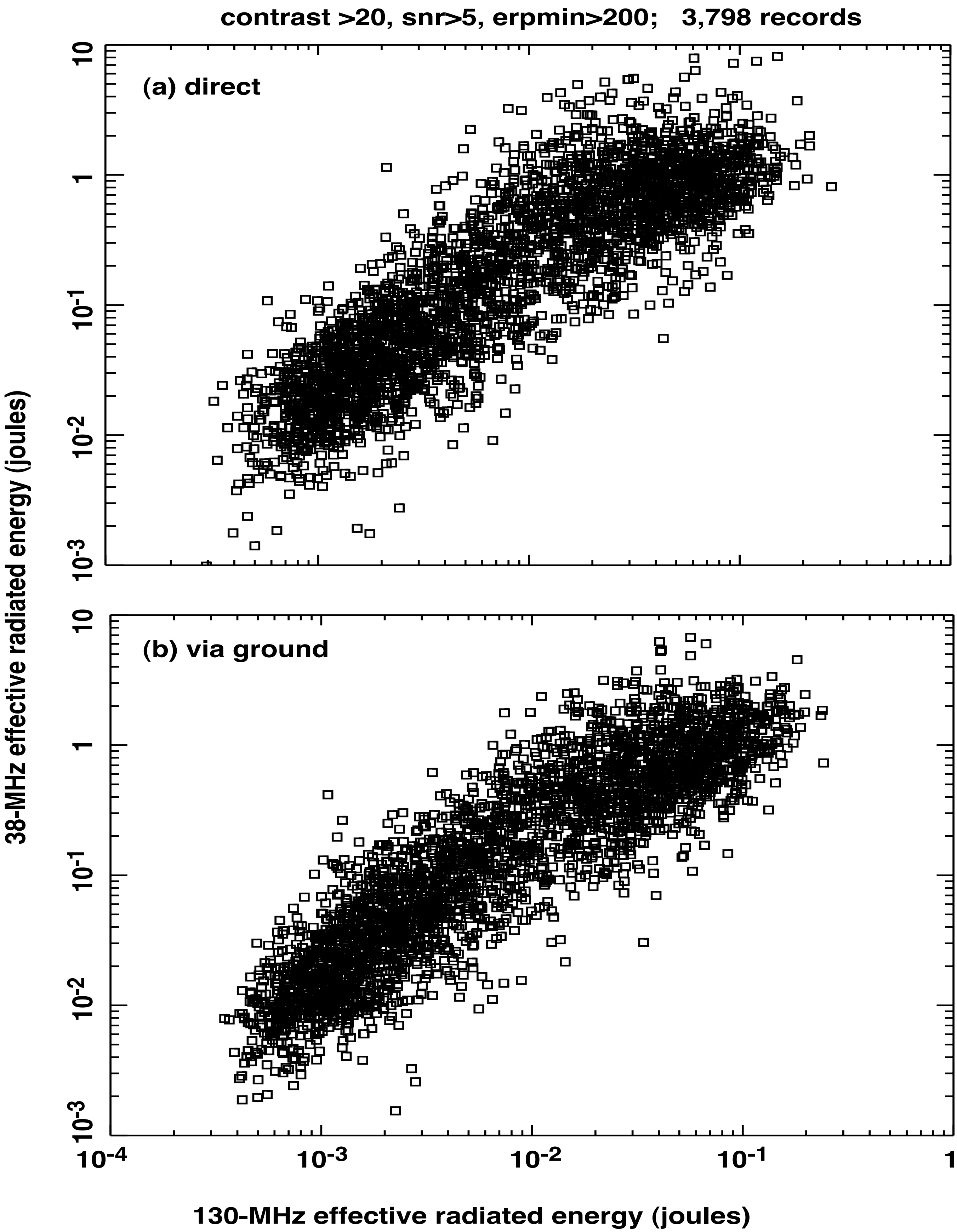

Figure 4: Scatter plot of effective radiated energy (J), using the less-stringent event set. Each point shows 38-MHz (vertical axis) vs 130-MHz (horizontal axis) energy of a pulse. (a) Direct path. (b) Path via ground.

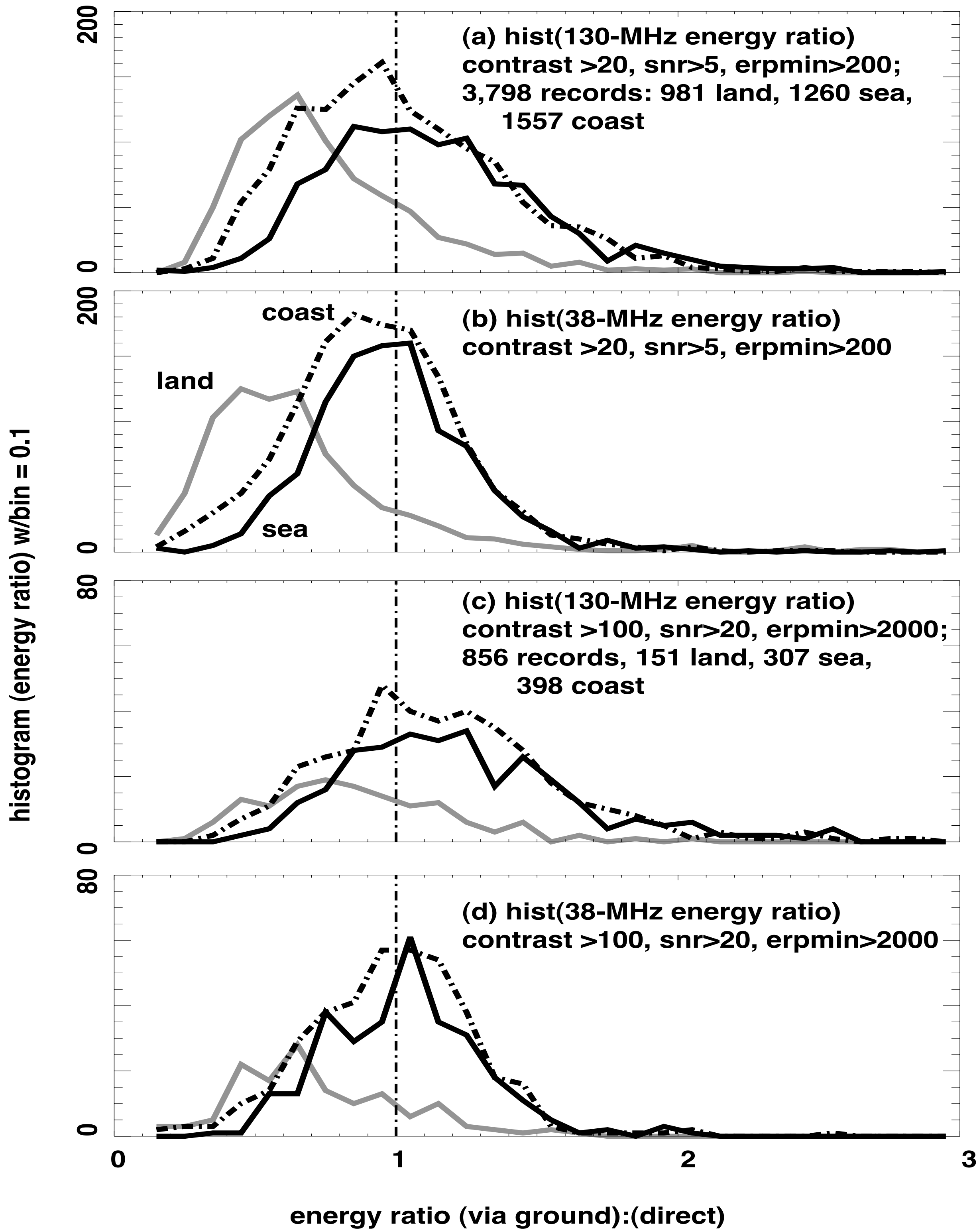

Figure 5: Histograms of (via ground)/(direct) pulse-energy ratio. Lightning locations separated according to being on sea (dark solid curve), coastal (dark dashed curve), and land (grey solid curve) areas. Vertical dashed line indicates unity energy ratio. (a) 130-MHz energy ratio, for less-stringent event set. (b) 38-MHz energy ratio, for less-stringent event set. (c) 130-MHz energy ratio, for more-stringent event set. (d) 38-MHz energy ratio, for more-stringent event set.

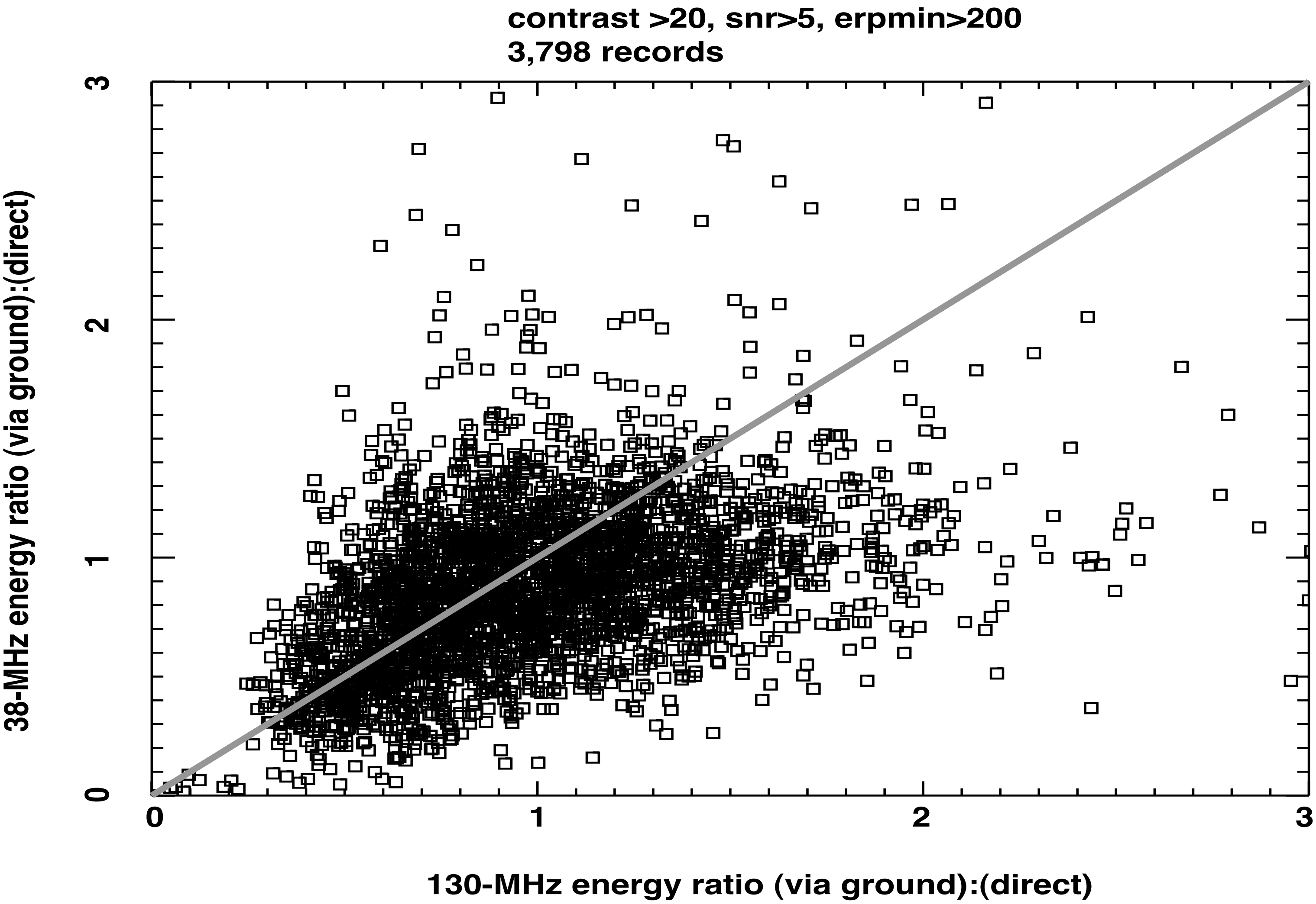

Figure 6: Scatter plot of 38-MHz (vertical axis) vs 130-MHz (horizontal axis) pulse-energy ratio (via ground)/(direct), using the less-stringent event set.

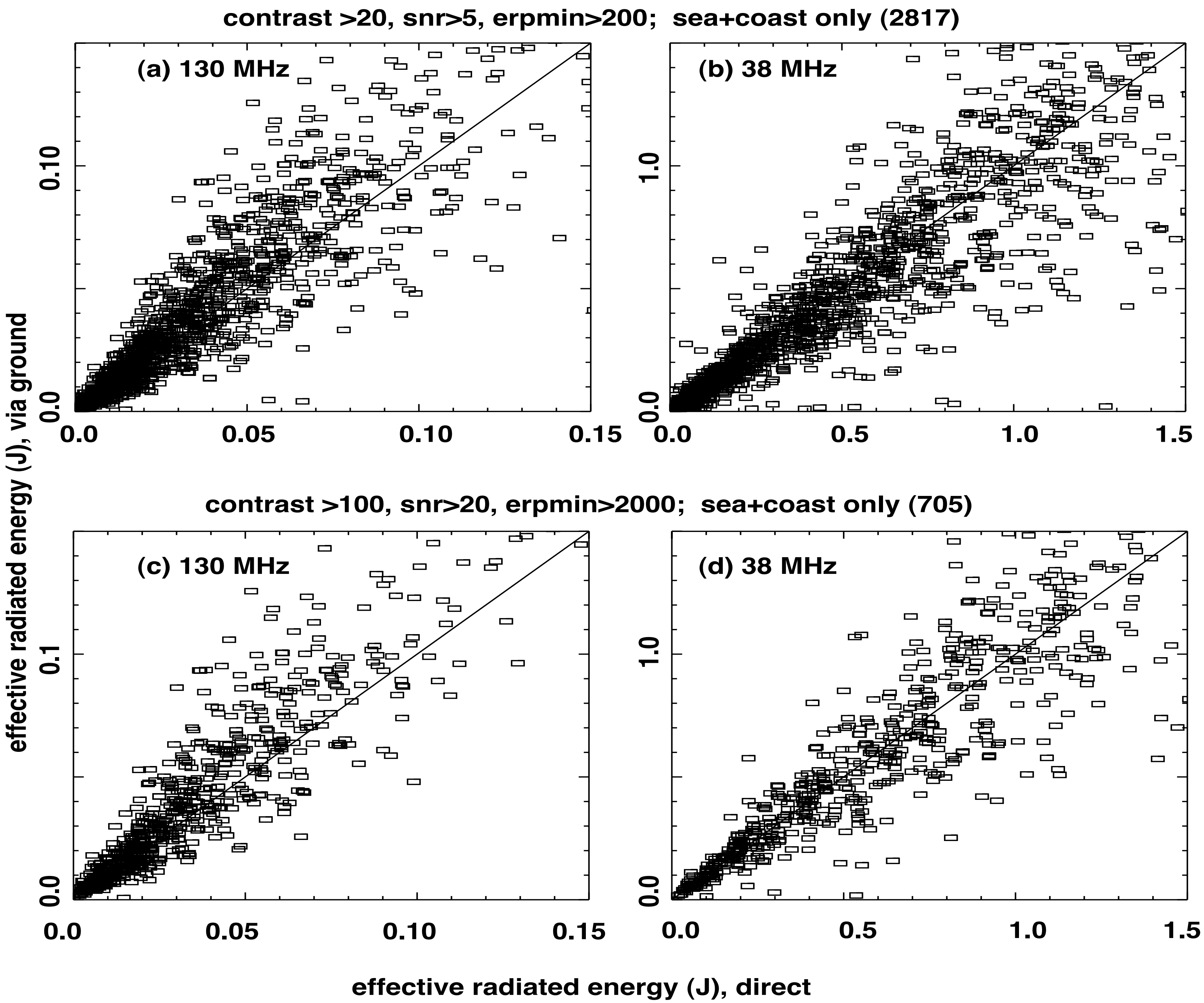

Figure 7: Scatter plots of effective radiated energy for path via ground (vertical axis) vs direct path (horizontal axis). Panels on left (a, c) are for 130 MHz, while panels on right (b, d) are for 38 MHz. Top two panels (a, b) are for all 2817 sea+coastal pulses within the less-stringent event set, while the bottom two panels are for all 705 sea+coastal pulses within the more-stringent event set.

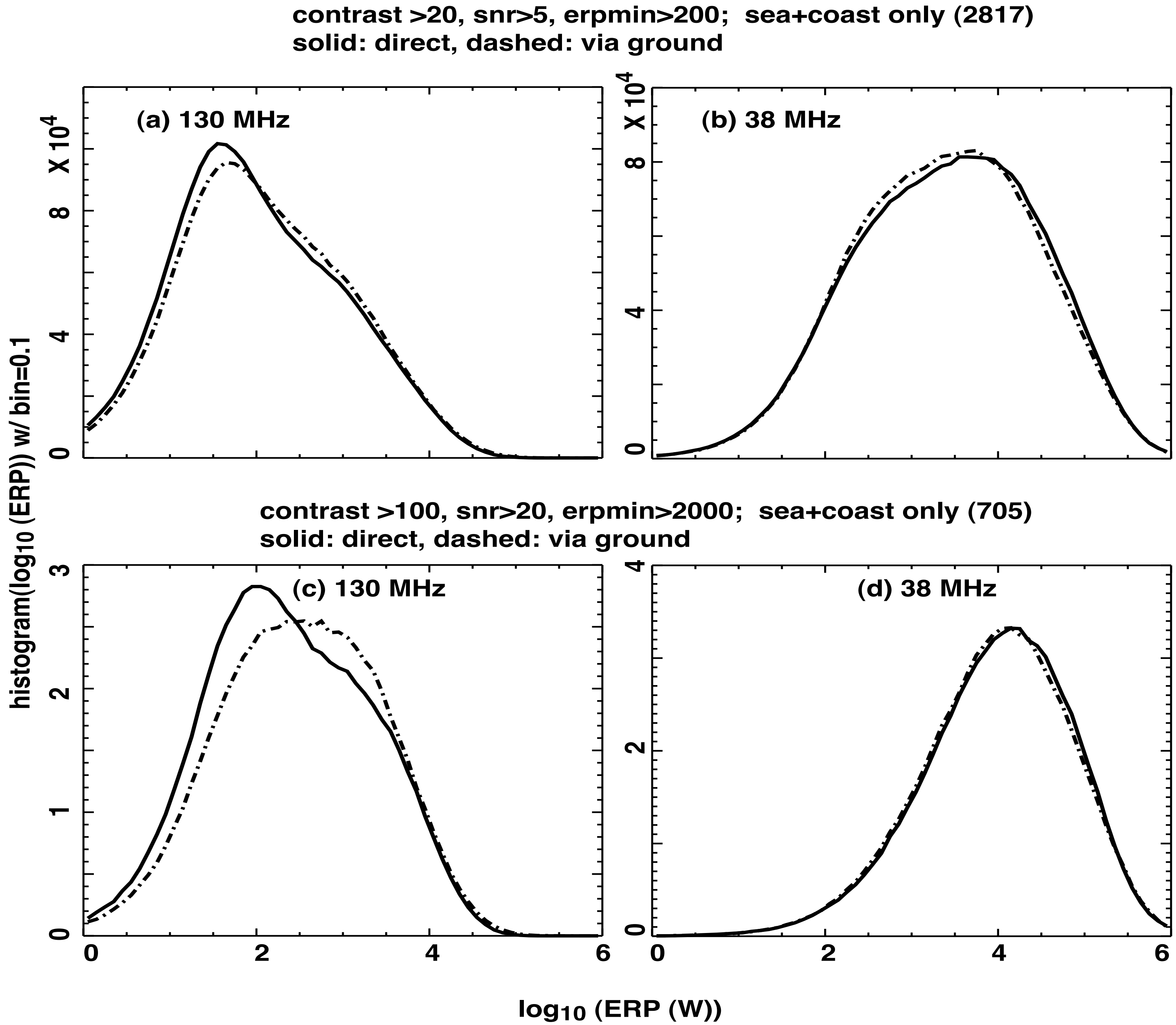

Figure 8: Histograms of instantaneous log10 (ERP) for (a, c) 130 MHz on left and for (b, d) 38 MHz on right. Top two panels (a, b) are for all 2817 sea+coastal pulses within the less-stringent event set, while the bottom two panels (c, d) are for all 705 sea+coastal pulses within the more-stringent event set. Solid curve: direct path; dashed curve: path via ground.

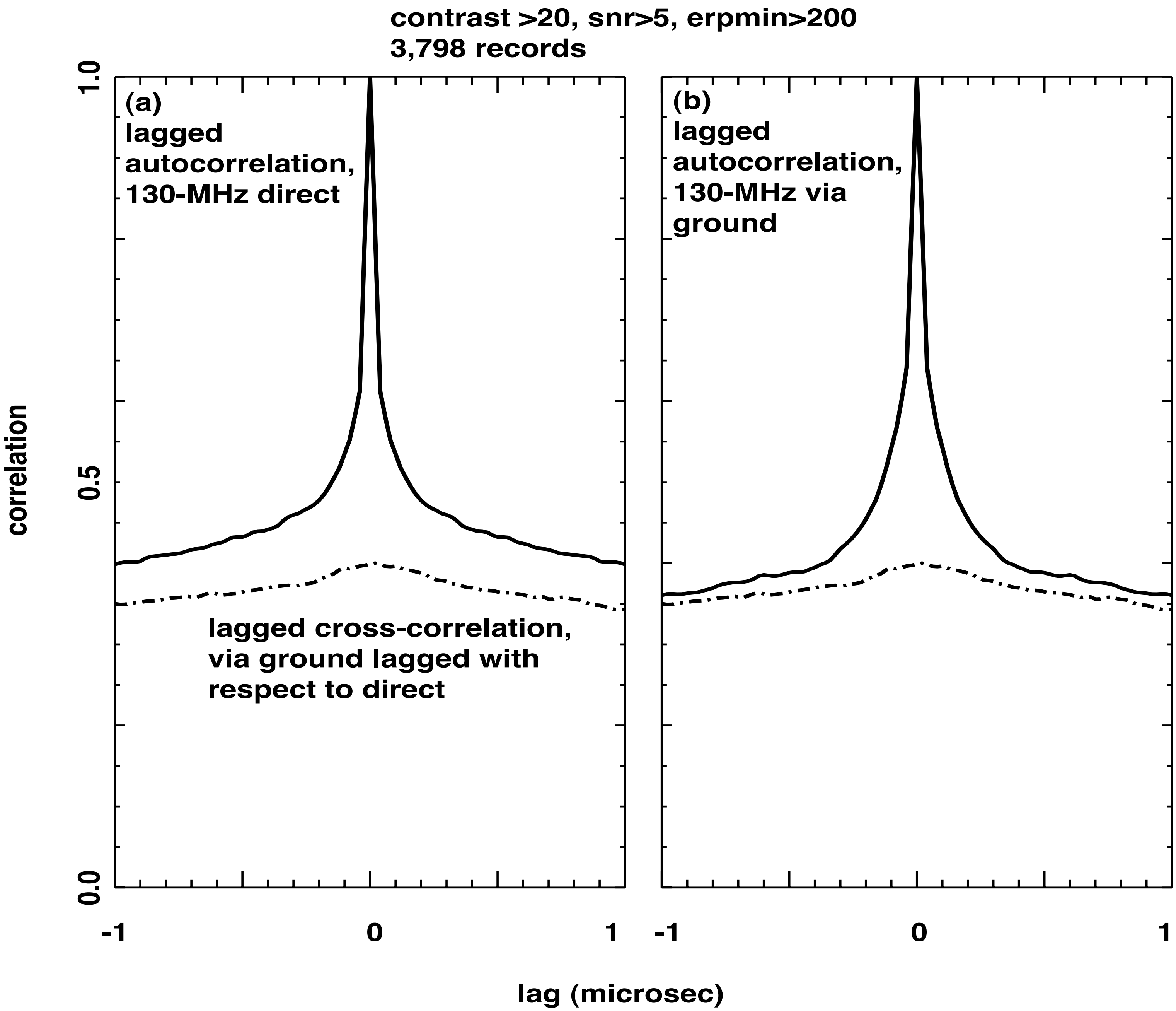

Figure 9: Lagged autocorrelation (solid curve) of instantaneous 130-MHz ERP, for (a) direct path and (b) path via ground, using all events in the less-stringent event. Dashed curve is the lagged cross-correlation of the path via ground with respect to the direct path, after syncronizing the pulse start of the two paths for each event record.

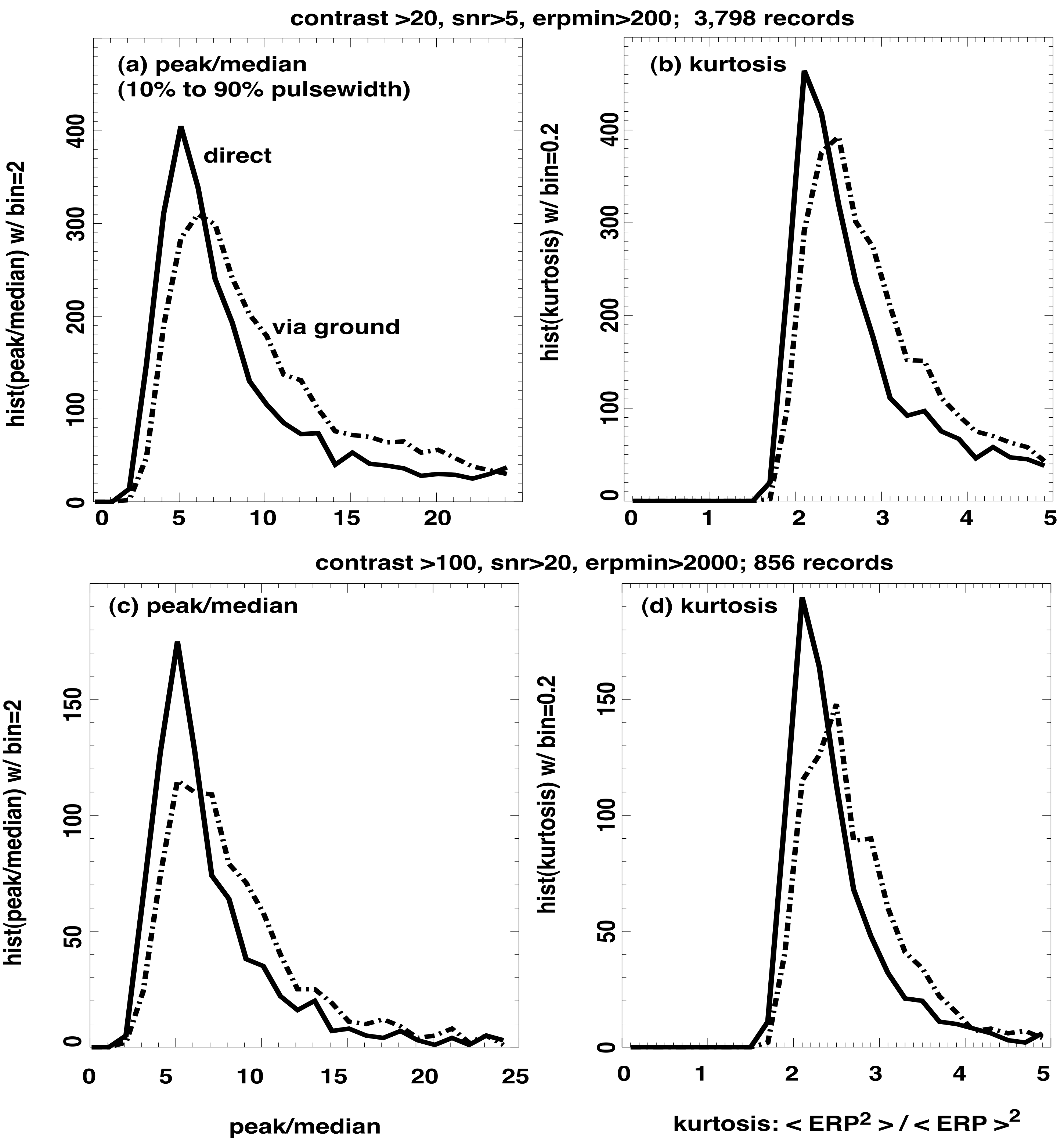

Figure 10: Histograms of (a, c) the ratio of peak/median ERP, and (b, d) the kurtosis of electric-field envelope, for 130-MHz pulses. Top row (a, b) is for the less-stringent event set, while bottom row (c, d) is for the more-stringent event set. Solid curve: Direct path; dashed curve: path via ground.

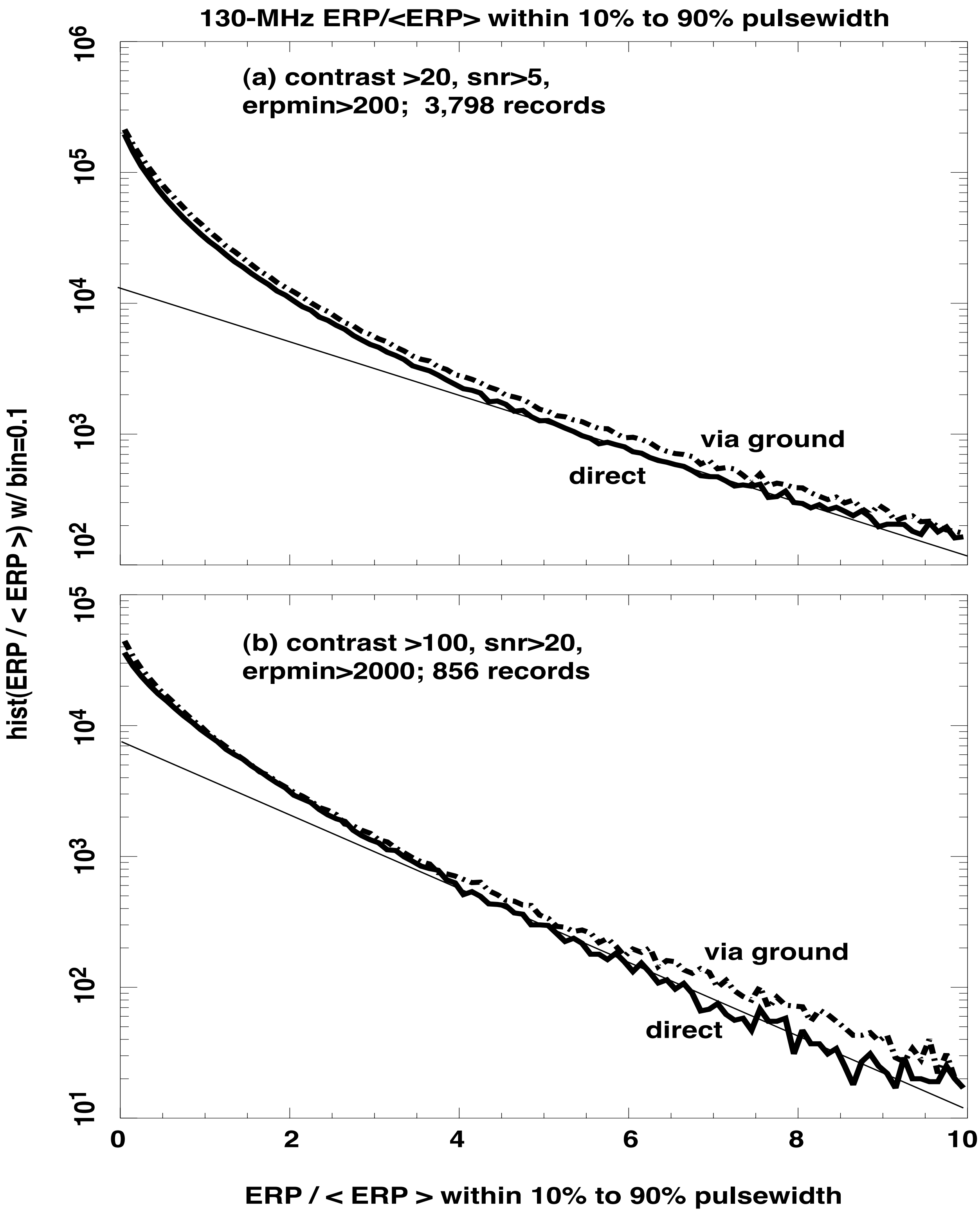

Figure 11: Histogram of the ratio of instantaneous ERP to pulse-averaged <ERP>, for (a) the less-stringent event set, and (b) the more-stringent event set. Heavy solid curve: direct path; heavy dashed curve: path via ground. Light solid tangent line: Rayleigh-fading behavior. Note the logarithmic vertical scale. An ERP-ratio statistic is accumulated each 0.02 microsec within the 10%-to-90% pulse duration.

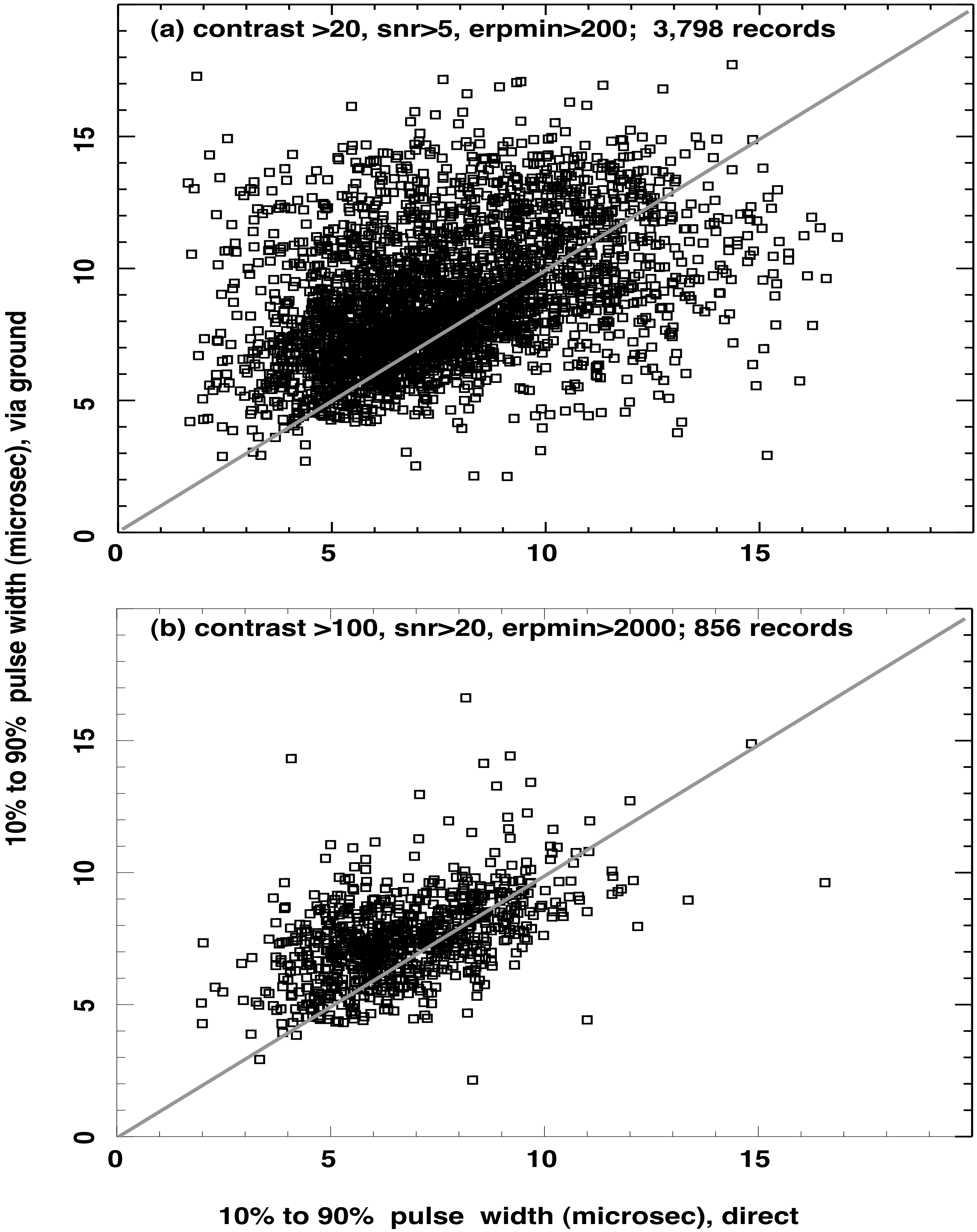

Figure 12: Scatter plots of 10%-to-90% pulse width at 130 MHz, for path via ground (vertical axis) vs direct path (horizontal axis). Grey line is for equality of the two. (a) Less-stringent event set. (b) More-stringent event set.

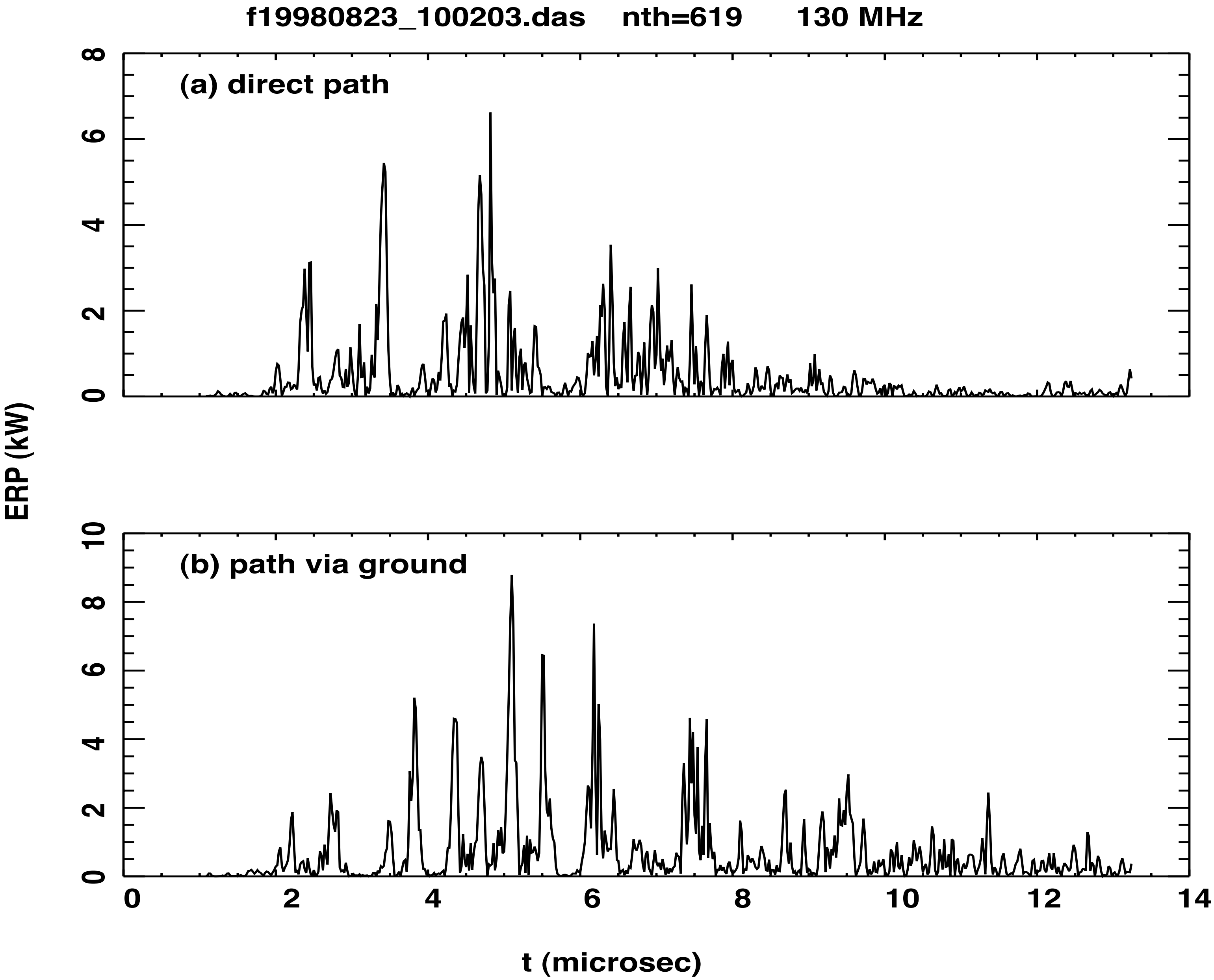

Figure 13: 130-MHz ERP vs time for event nth=619 within file f19980823_100203.das. (a) Direct path. (b) Path via ground. The signals have been aligned to syncronize their leading rise as best as possible, and only 14 microsec are shown for each propagation path.

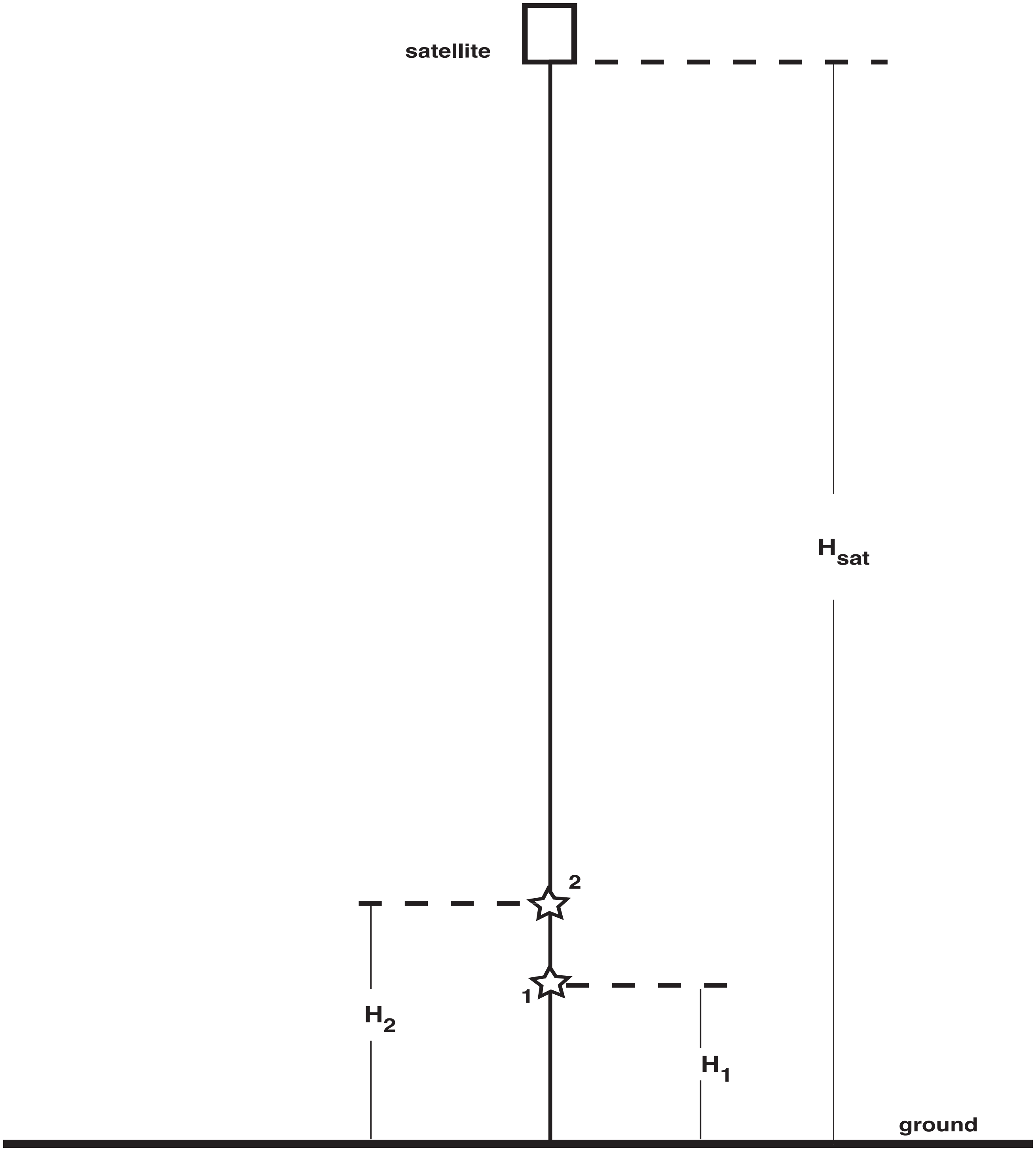

Figure 14: Simple one-dimensional case of a spatially-separated pair of discharge elements, at heights H_1 and H_2, along the satellite nadir axis.